Optogenetic toolkit reveals the role of Ca^{2+} sparklets in coordinated cell migration

Jin Man Kim[a,b,1], Minji Lee[c,1], Nury Kim[d], and Won Do Heo[c,d,e,2]

[a]Graduate School of Medical Science and Engineering, Korea Advanced Institute of Science and Technology (KAIST), Daejeon 34141, Republic of Korea; [b]Department of Physiology, School of Dentistry, Seoul National University and Dental Research Institute, Seoul 03080, Republic of Korea; [c]Department of Biological Sciences, KAIST, Daejeon 34141, Republic of Korea; [d]Center for Cognition and Sociality, Institute for Basic Science, Daejeon 34141, Republic of Korea; and [e]KAIST Institute for the BioCentury, KAIST, Daejeon 34141, Republic of Korea

Edited by Peter N. Devreotes, The Johns Hopkins University School of Medicine, Baltimore, MD, and approved April 19, 2016 (received for review September 16, 2015)

Cell migration is controlled by various Ca^{2+} signals. Local Ca^{2+} signals, in particular, have been identified as versatile modulators of cell migration because of their spatiotemporal diversity. However, little is known about how local Ca^{2+} signals coordinate between the front and rear regions in directionally migrating cells. Here, we elucidate the spatial role of local Ca^{2+} signals in directed cell migration through combinatorial application of an optogenetic toolkit. An optically guided cell migration approach revealed the existence of Ca^{2+} sparklets mediated by L-type voltage-dependent Ca^{2+} channels in the rear part of migrating cells. Notably, we found that this locally concentrated Ca^{2+} influx acts as an essential transducer in establishing a global front-to-rear increasing Ca^{2+} gradient. This asymmetrical Ca^{2+} gradient is crucial for maintaining front–rear morphological polarity by restricting spontaneous lamellipodia formation in the rear part of migrating cells. Collectively, our findings demonstrate a clear link between local Ca^{2+} sparklets and front–rear coordination during directed cell migration.

optogenetics | cell migration | calcium signaling | cell polarity | actin cytoskeleton

Mesenchymal cell migration is characterized by polarization of the cell to form a leading edge with adhesive-mediated protrusion and a trailing edge with a contractile cell rear (1). To maintain their polarized morphology and achieve efficient migration, migrating cells require front–rear coordination: simultaneous harmonization of frontal protrusion and rear retraction. This coordination is a key process in directional cell migration and is regulated by diverse external guidance cues that steer intrinsic cell directionality (2). Among intracellular signaling messengers, Ca^{2+} signals are widely known to regulate cell migration. Intracellular Ca^{2+} signals are fine tuned in space and time by intracellular Ca^{2+} buffers and reservoirs (3). Given their spatiotemporal diversity, localized Ca^{2+} signals act as versatile signaling mediators of the functions that constitute the multiple steps in cell movement. For example, localized Ca^{2+} influx derived from stretch-activated Ca^{2+} channels in the front region of migrating cells is known to steer membrane protrusions (4). Moreover, other types of Ca^{2+} influxes have been reported to mediate detachment of the trailing part of the cell during migration (5, 6). Although such reports regarding local Ca^{2+} effects have provided fragmentary insight into the motile processes, how these local Ca^{2+} signals systemically operate to coordinate cell migration is still incompletely understood.

As knowledge about cell migration has grown, so too have demands for novel approaches capable of recapitulating cellular movements with the precise spatiotemporal resolution necessary to accurately dissect mechanisms underlying directional migration (2). A variety of optogenetic tools based on light-controllable proteins have recently been introduced as a means for regulating biological activity in living cells and organisms (7–9). This notable expansion of optogenetics has opened up new avenues for regulating diverse signaling pathways in a robust, reversible, and spatiotemporal manner (10). In particular, recently developed optogenetic tools have demonstrated remarkable efficacy in controlling cell motility and related signals through tailored optical input (7, 11). Exploiting the photosensory protein cryptochrome 2 of *Arabidopsis thaliana*, we recently developed an optically controllable receptor tyrosine kinase (RTK), optically controlled FGF receptor 1 (optoFGFR1), and demonstrated its precise spatiotemporal regulation of cell polarity and directionality (12). Such versatile regulators of cell motility have the potential to unveil the mechanisms underlying directional cell migration, which are difficult to address using previously existing methods.

Here, using optogenetic tools that modulate RTK downstream pathways, we elucidated the spatially distinct role of local Ca^{2+} signals in directed cell migration. With this toolkit, we were able to visualize locally evoked Ca^{2+} sparklets, which are crucial for coordinated migration of endothelial cells through induction of a polarized state. Notably, this Ca^{2+} influx establishes a front-to-rear increasing Ca^{2+} gradient in migrating cells that consequently maintains cell polarity by restricting spontaneous lamellipodia formation in the trailing edge. This study identifies a previously unrecognized pathway that links Ca^{2+} sparklets, Ca^{2+} gradients, and front–rear coordination in the context of directed cell migration.

Results

The Effect of RTK Downstream Pathways in Coordinated Migration. RTK signaling pathway plays a central role in connecting ligand (signaling input) to migration (functional output) in cells that directionally migrate in response to external cues. To determine the different contributions of each signaling node of RTK downstream to the process of directed cell migration, we used

Significance

In this article, we present a pioneering experimental approach for studying cell migration and more broadly establish representative guidelines for applying an optogenetic approach in biological studies. Using recently developed optogenetic tools, we identified local Ca^{2+} influx as a major source of Ca^{2+} for gradient formation and established the functional importance of polarized chemistry in highly coordinated cell migration. These findings provide strong evidence for a mechanism that addresses fundamental questions about front–rear Ca^{2+} gradients in migrating cells and suggest a previously unidentified role of voltage-dependent Ca^{2+} channels in the directional migration of nonexcitable cells.

Author contributions: J.M.K., M.L., N.K., and W.D.H. designed research; J.M.K. and M.L. performed research; J.M.K. contributed new reagents/analytic tools; J.M.K., M.L., N.K., and W.D.H. analyzed data; and J.M.K., M.L., N.K., and W.D.H. wrote the paper.

The authors declare no conflict of interest.

This article is a PNAS Direct Submission.

[1]J.M.K. and M.L. contributed equally to this work.

[2]To whom correspondence should be addressed. Email: wdheo@kaist.ac.kr.

This article contains supporting information online at www.pnas.org/lookup/suppl/doi:10.1073/pnas.1518412113/-/DCSupplemental.

two optogenetic tools—optically controlled fibroblast growth factor receptor 1 (optoFGFR1) (12) and photoactivatable Rho small GTPase Rac1 (PA-Rac1) (7)—which optically regulate cell migration by activating distinct nodes in the signaling hierarchy (Fig. 1*A*). Each optogenetic tool was expressed in human umbilical vein endothelial cells (HUVECs), and the motile pattern guided by localized photoactivation was monitored. In both cases, localized illumination (488 nm, 1 μW, 15-s intervals) oriented the leading edge toward the illuminated area with increasing membrane protrusion (optoFGFR1: +18.2%; PA-Rac1: +17.7%, relative to entire cell area; Fig. 1 *B* and *C*). However, significantly more retraction on the opposite side of illumination was observed in optoFGFR1-expressing cells (−27.1%) compared with PA-Rac1–expressing cells (−15.9%; $P = 0.032$) (Fig. 1*D* and Fig. S1 *A* and *B*). Based on this optically oriented direction of cell movement, we defined the illuminated part as "front" and the opposite part as "rear." We then investigated signal dynamics of Lifeact (F-actin biosensor) (13) in HUVECs during optical guidance. Overall Lifeact signals in the front region gradually decreased in both groups, indicating actin turnover from thick fiber to branched form during lamellipodia formation; whereas only optoFGFR1-expressing cell showed remarkable local accumulation of Lifeact signals in the contracting rear region, indicating stress fiber formation, in accordance with our previous finding (12) (Fig. 1 *E*–*H*). A graph quantifying Lifeact intensity clearly showed the increasing pattern (+46.5%) in the rear part of optoFGFR1-expressing HUVECs (Fig. S1 *C*–*E*). We also observed that myosin signals [myosin regulatory light chain 2 (MRLC2)-iRFP682] were preferentially colocalized with the accumulated Lifeact signals, implying that actomyosin crosslinking drives rear retraction during optical guidance of HUVECs (Fig. S1 *F* and *G*). Such rear myosin concentration is also known to coordinate cell motility through organization of front–rear actin network treadmilling (14). Collectively, these results demonstrate the hierarchical difference of signals in front–rear coordinated cell migration, represented by harmonization of rear retraction with frontal protrusion: upstream RTK induces more robust retraction than downstream Rac1. In the case of PA-Rac1, retraction occurred with prolonged photoactivation (90 min), indicating that PA-Rac1 also leads to coordination rather than simply producing frontal protrusion (Fig. S1*H*).

Identifying Local Ca^{2+} Signals in Migrating HUVECs. We hypothesized that the observed rear retraction might be related to the local Ca^{2+} distribution, a factor well known to generate cell contractility (15). To test this, we first modified red fluorescent genetically encoded calcium indicators for optical imaging version 1 (R-GECO1) (16), an intensiometric Ca^{2+} biosensor, to produce a membrane-tethered format (Lyn-R-GECO1) to increase sensitivity and spatial resolution of the biosensor (17). We then cotransfected Lyn-R-GECO1 and

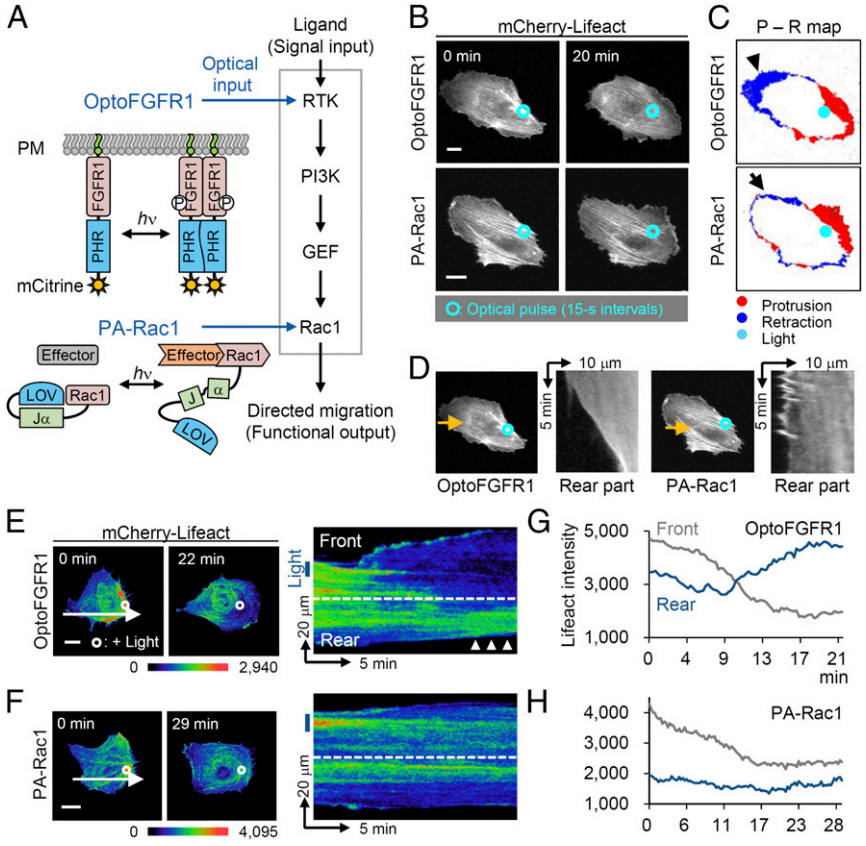

Fig. 1. Hierarchically different effects of RTK downstream signaling on front–rear coordination. (*A*) Schematic representation of optoFGFR1 and photoactivatable Rac1 (PA-Rac1, *Left*) and their application to simplified RTK downstream signaling (*Right*). FGFR1, cytoplasmic region of FGFR1; PHR, photolyase homology region of cryptochrome 2; LOV, light oxygen voltage domain from phototropin1; Jα, α-helical extension of phototropin1. (*B*) Lifeact (F-actin biosensor) images of HUVECs undergoing subcellular activation of optoFGFR1 (*Upper*) and PA-Rac1 (*Lower*) by local illumination (blue circles, 488 nm, 1 μW, 15-s intervals). (*C*) Protrusion retraction maps of optically guided HUVECs. Arrowhead and arrow indicate the retracting part of cells expressing optoFGFR1 and PA-Rac1, respectively. (*D*) Kymographs of the rear part of the cells in *B*. Yellow arrows represent the line-scanned area. (*E* and *F*) Pseudocolored Lifeact (F-actin biosensor) images (*Left*) and kymograph (*Right*) of optically guided HUVECs. White circles and blue boxes indicate illuminated regions; white arrows indicate line-scanned area; arrowheads indicate accumulation of Lifeact signals. (*G* and *H*) Quantified intensity of Lifeact signal in front and rear parts of the cells in *E* and *F*. (Scale bars: 20 μm.)

optoFGFR1 into HUVECs and monitored local Ca^{2+} dynamics during optically guided cell movement. Upon local activation of optoFGFR1, two distinct patterns of Lyn-R-GECO1–based Ca^{2+} geometry were clearly visible: Ca^{2+} puffs, broad (mean width: 48.09 μm), oscillating signals localized around the illuminated area; and Ca^{2+} sparklets, pinpoint signals (4.03 μm) detected in the light-unreachable peripheral region of the cell (18) (Fig. 2 *A–C* and Movie S1). By contrast, local activation of PA-Rac1 did not induce remarkable changes in Ca^{2+} levels (Fig. S2*A*). We then investigated the spatiotemporal characteristics of Ca^{2+} sparklets, including distribution, amplitude, and duration in multiple cells (Fig. S2 *B–D*). Notably, Ca^{2+} sparklets were predominantly (65.4%) located in the rear retracting part of migrating HUVECs (Fig. 2*D*). Upon addition of serum instead of optical stimulation, sparklets were also observed near the retracting part of migrating cells (Fig. S2 *E* and *F*). These data suggest the possibility that Ca^{2+} sparklets are related to the rear retraction in migrating HUVECs.

Next, to identify the origin of Ca^{2+} sparklets, we monitored their frequency in HUVECs treated with various Ca^{2+} antagonists during optically guided cell movement. Control (untreated) cells exhibited a Ca^{2+} sparklet frequency of 0.442 mHz (per 100 μm^2 cell area) (Fig. 2*E*). EGTA treatment almost completely blocked these signals (0.018 mHz), confirming their dependence on the influx of Ca^{2+} from the external environment (Fig. 2*E* and Fig. S2*G*). Among

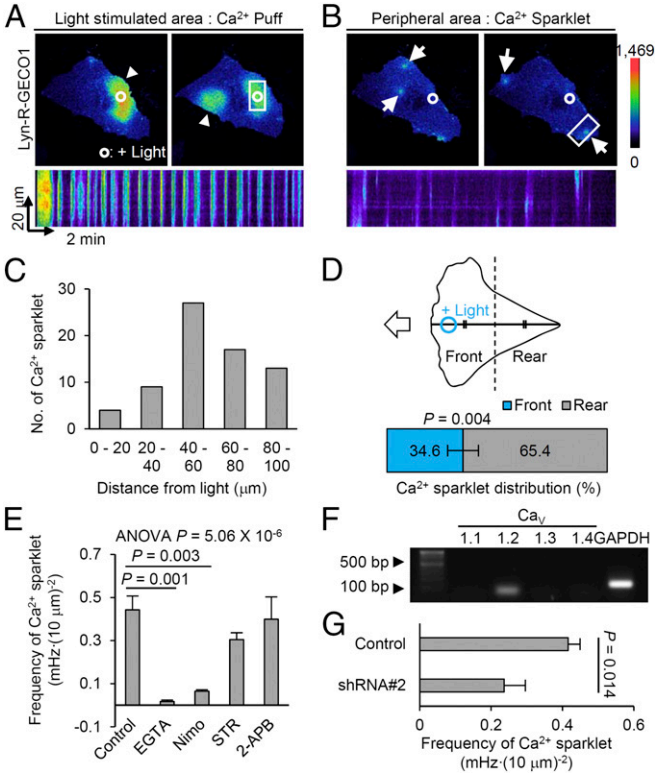

Fig. 2. Distinct Ca^{2+} patterns induced by subcellular activation of optoFGFR1. (*A* and *B*) (*Upper*) Pseudocolored images of Lyn-R-GECO1 (membrane-targeted Ca^{2+} sensor) showing Ca^{2+} puffs (arrowheads) and Ca^{2+} sparklets (arrows). (*Lower*) Kymographs scanning white-squared region. (Magnification: 60×.) (*C*) Distribution of Ca^{2+} sparklets of *B* in relation to distance from the illuminated region. (*D*) The front–rear distribution of Ca^{2+} sparklets in HUVECs optically guided by optoFGFR1. $n = 8$, mean ± SEM, two-tailed *t* test. (*E*) Frequency of Ca^{2+} sparklets in HUVECs treated with various inhibitors. Nimo, nimodipine; STR, streptomycin; 2-APB, 2-aminoethoxydiphenyl borate. $n > 7$, mean ± SEM, one-way ANOVA. One outlier was excluded. (*F*) mRNA expression profile of L-type Ca_V channel subtypes in HUVECs. (*G*) Frequency of Ca^{2+} sparklets in HUVECs transfected with shRNA ($Ca_V1.2$ knockdown). $n = 11$, mean ± SEM, two-tailed *t* test.

Ca^{2+} channel inhibitors tested, only nimodipine, an L-type voltage-dependent Ca^{2+} (Ca_V) channel inhibitor, significantly blocked Ca^{2+} sparklets (0.065 mHz) without affecting Ca^{2+} puff generation (Fig. 2*E* and Fig. S2*G*). A similar Ca^{2+} pattern was also observed in the human breast cancer cell line MDA-MB-231 under the same optical-stimulation conditions (Fig. S2*H*), suggesting the broad implication of Ca^{2+} sparklets in different biological contexts. We then identified predominant expression of $Ca_V1.2$ among L-type Ca_V channel subtypes ($Ca_V1.1$–1.4) (19) in HUVECs (Fig. 2*F*), and also observed significantly decreased frequency of Ca^{2+} sparklets by translational knockdown of $Ca_V1.2$ by transfecting short hairpin RNA (shRNA) plasmid (Fig. 2*G* and Fig. S2*I*). These data demonstrate that $Ca_V1.2$ mediates the observed Ca^{2+} sparklets.

Elucidating the Ca^{2+} Sparklet-Related Signaling Network. Which signaling pathway is the key inducer of Ca^{2+} sparklets? Among various RTK downstreams, the phosphoinositide 3-kinase (PI3K) pathway has been suggested to regulate Ca_V channel activity by changing the lipid composition of the cell membrane (20, 21). In support of this possibility, treatment with LY294002 (PI3K inhibitor) markedly inhibited Ca^{2+} sparklets in HUVECs optically guided by optoFGFR1 (Fig. S3*A*). We then applied light-inducible PI3K (11) (Fig. S3*B*) to verify the individual action of the PI3K signaling node on evoking Ca^{2+} sparklets in optically guided HUVECs. Local activation of light-inducible PI3K clearly evoked Ca^{2+} sparklets with a frequency (0.447 mHz) similar to that in optoFGFR1-expressing cells (0.442 mHz) in association with reduced Ca^{2+} puff activity (Fig. S3*C*). Next, we investigated whether membrane lipid modulation by PI3K is involved in evoking Ca^{2+} sparklets and, if so, which PI component is crucial. To this end, we overexpressed pleckstrin homology (PH) domains, which bind to 3-phosphorylated PIs (3-PIs) [$PI(3,4)P_2$ or $PI(3,4,5)P_3$], in HUVECs to prevent the interaction between 3-PIs and other effectors, and measured the frequency of Ca^{2+} sparklets during optical guidance by optoFGFR1 (Fig. S3*D*). We found that all PH domains that bind 3-PIs reduced the frequency of Ca^{2+} sparklets to basal levels (Fig. S3*E*). These results demonstrate the importance of membrane lipid modulation by the PI3K pathway in evoking Ca^{2+} sparklets.

Next, we investigated the mechanism underlying the concentrated localization of Ca^{2+} sparklets in the rear part of migrating cells (Fig. 2 *C* and *D*). As shown in Fig. S3 *A–E*, it is clear that the FGFR–PI3K–3-PI signaling axis increases the frequency of Ca^{2+} sparklets above the basal level. In the case of partial activation of optoFGFR1, which mimics a situation in which cells move toward a chemical attractant, we anticipated that 3-PIs generated from the illuminated (front) area could affect membrane lipid composition in the rear part through rapid diffusion through the plasma membrane, owing to their high diffusion coefficient (0.5–2 $\mu m^2/s$) (22, 23). Consequently, the diffused 3-PIs may act as enhancers of Ca^{2+} sparklets in the rear part of HUVECs. If this is the case, why are Ca^{2+} sparklets down-regulated in the front area of the cell? We hypothesized that there is a dominant Ca^{2+} sparklet-inhibitory signal in the FGFR-activated front region. Among the various downstream signaling pathways engaged by FGFR, we found that protein kinase C (PKC) activation by phorbol 12-myristate 13-acetate (PMA) treatment dramatically suppressed Ca^{2+} sparklets (Fig. S3*F*). This suppressive effect was also observed in PKC-overexpressing cells (Fig. S3*G*). Classic PKC isoforms are known to regulate L-type Ca_V channel activity through diverse receptor-mediated signaling pathways (24, 25). We also observed PKC recruitment in the front region where optoFGFR1 was locally activated, a response that was absent in cells expressing the PLCγ-binding–deficient optoFGFR1 mutant, Y766F (Fig. S3 *H* and *I*). Consistent with this, the PKC inhibitor Gö6983 significantly increased the proportion of Ca^{2+} sparklets in the front region of optically guided HUVECs (Fig. S3*J*), indicating that PKC is a major repressor of Ca^{2+} sparklets in the front region. Collectively, these findings suggest that diffusion of 3-PIs from

the illuminated region might enhance the activity of Ca_V channels in the rear part, and that Ca_V channels in the front region are simultaneously inhibited by activated PKC (Fig. S3*K*). This proposed model of signaling coupling between PI3K and PKC provides a plausible explanation for the posteriorly concentrated distribution of Ca^{2+} sparklets.

Which signaling pathway is involved in Ca^{2+}-mediated retraction? During muscle/nonmuscle cell contraction, elevated intracellular Ca^{2+} mediates actomyosin contraction through the calmodulin-dependent myosin light chain kinase (MLCK) signaling pathway (26). Therefore, we evaluated changes in phosphorylated MLC (pMLC) levels induced by treatment of HUVECs with basic fibroblast growth factor (bFGF) in the presence and absence of nimodipine. Immunofluorescence results showed that bFGF increased pMLC levels by 13.4%, and the effect was completely inhibited by preincubation (1 h) with nimodipine (Fig. S4 *A* and *B*). Additionally, HUVECs coexpressing kinase-dead MLCK (MLCK-KD) exhibited impaired trailing-edge contraction during optical guidance by optoFGFR1. A similar motile pattern was also observed after nimodipine treatment (Fig. S4 *C* and *D*). These results demonstrate that the MLCK pathway is a major signaling mediator of the rear retraction of migrating cells.

Ca^{2+} Sparklets Establish a Front–Rear Ca^{2+} Gradient. A front-to-rear increasing global Ca^{2+} gradient during directed cell migration has been extensively reported in diverse cell types (4, 27, 28). We speculated that Ca^{2+} sparklets contribute to establishing the Ca^{2+} gradient owing to their spatial concentration in the rear part (Fig. 2 *C* and *D*). To support this conjecture, we first confirmed a front-to-rear increasing Ca^{2+} gradient in directionally migrating HUVECs in a polarized state under serum-supplemented condition using ratiometric Ca^{2+} measurements (Fluo-4/Fura Red) (29) (Fig. S5 *A* and *B*). The method for detecting Ca^{2+} gradient in our system was validated by demonstrating the presence of a Ca^{2+} gradient in WI-38 (Wistar Institute 38) human fetal lung fibroblasts (Fig. S5 *A* and *B*) known to possess an overtly polarized morphology and Ca^{2+} gradient (4). We could not guide cells with optogenetic tools under the imaging conditions used for ratiometric Ca^{2+} measurements, because the method requires excitation by multichannels of laser, including the wavelength used to activate optogenetic modules (~488 nm). Therefore, we selected migrating HUVECs that retained a well-established Ca^{2+} gradient and polarized morphology and monitored changes in the gradient upon inhibition of Ca_V channels. Surprisingly, nimodipine treatment immediately equalized the Ca^{2+} gradient; by contrast, vehicle (DMSO)-treated cells maintained their rear-increased Ca^{2+} gradient (Fig. 3 *A*–*D*). Additionally, we confirmed that extracellular Ca^{2+} chelation with EGTA also decreased the steepness of the Ca^{2+} gradient (Fig. S6*A*), supporting the conclusion that Ca^{2+} influx via Ca_V channels in the form of Ca^{2+} sparklets is a major player in modulating the intracellular Ca^{2+} gradient.

Next, to demonstrate the relationship between the Ca^{2+} sparklets and the front–rear gradient, we tested whether local Ca^{2+} sparklets can modulate global Ca^{2+} levels. To conditionally evoke Ca^{2+} sparklets, we applied chemically inducible PI3K (30, 31), which generates 3-PIs upon treatment with the chemical dimerizer, rapamycin. Using the membrane-tethered Ca^{2+} biosensor, Lyn-R-GECO1, we confirmed that 3-PIs generated by rapamycin treatment dramatically increased the frequency of local Ca^{2+} sparklets in HUVECs without inducing Ca^{2+} puffs (Fig. S6*C*). Using the same conditions except replacing Lyn-R-GECO1 with R-GECO1, which is better suited to visualizing global $[Ca^{2+}]_i$ changes, owing to its cytoplasmic location and higher diffusion rate (Fig. S6*B*), we observed that rapamycin treatment remarkably increased global Ca^{2+} levels (Fig. S6 *D* and *E*). Notably, combined treatment with rapamycin and nimodipine almost completely abolished this increase, and treatment with nimodipine alone significantly decreased basal Ca^{2+} levels ($P = 2.0 \times 10^{-4}$; Fig. S6 *D* and *E*). These data indicate that local Ca^{2+} sparklets mediated by Ca_V channels can modulate global Ca^{2+} levels, and thus provide indirect, but strong, evidence demonstrating the role of asymmetric sparklets in generating global Ca^{2+} gradients.

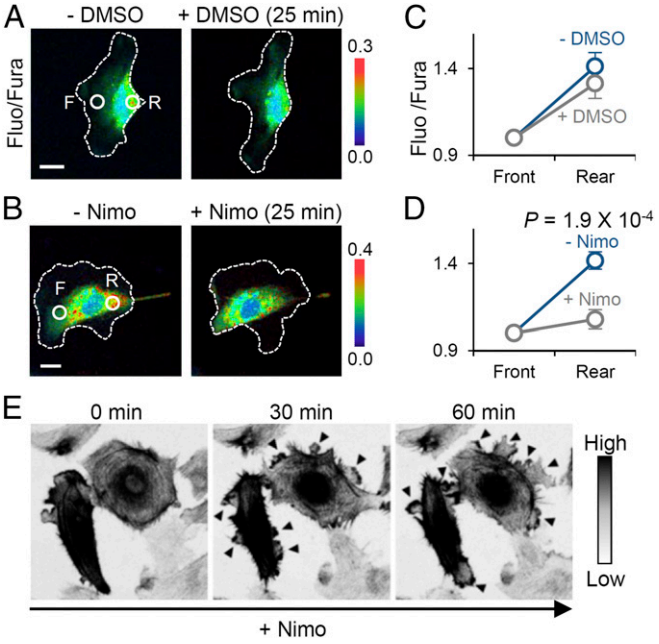

Fig. 3. Front-to-rear Ca^{2+} gradient and its role in maintaining cell polarity. (*A* and *B*) Fluo-4/Fura Red ratio images of a HUVEC before and after treatment with DMSO (*A*) or nimodipine (*B*). White dotted lines depict cell outline. F, front; R, rear. (*C* and *D*) Change in the steepness of the Ca^{2+} gradient after treatment with DMSO ($n = 9$) or nimodipine ($n = 9$). Data are represented as mean ± SEM, two-tailed *t* test. (*E*) Time-lapse images (inverted contrast) of mCherry-Lifeact–expressing HUVECs displaying the spontaneous lamellipodia protrusion after nimodipine treatment. Arrowheads indicate newly formed protrusions. (Scale bars: 20 μm.)

Next, we evaluated morphological changes of HUVECs following perturbation of Ca^{2+} gradients by nimodipine treatment. Immediately after nimodipine treatment, Lifeact-expressing HUVECs under serum-supplemented conditions displayed multiple and spontaneous protrusions along the entire cell edge (Fig. 3*E*). Regulated formation of lamellipodia is required for directionally persistent cell migration; conversely, increased numbers of lamellipodia reflect randomized directionality with reduced responsiveness to external cues (2). Applying this concept, these morphological changes could be interpreted to mean the Ca_V channel-mediated Ca^{2+} gradient is important for regulating cell directionality in directional migration.

Effects of the Ca_V Channel-Mediated Ca^{2+} Gradient on Directed Cell Migration. To dissect the function of the $Ca_V1.2$-mediated Ca^{2+} gradient in motile behavior in greater detail, we designed a "time-square model," which guides the reproducible migration of an individual cell through a standardized, square-shaped optical input (488 nm, 4 μW, 30-s intervals) with time-course live imaging (Fig. 4*A*). In the time-square model, optoFGFR1-expressing HUVECs exhibited well-defined leading and trailing edges that were thoroughly coordinated during migration toward the illuminated region (Fig. 4*B* and Movie S2). However, upon perturbing the Ca^{2+} distribution by nimodipine treatment, the direction of migrating HUVECs was frequently altered by spontaneous membrane protrusions from the trailing edge, resulting in unstable directionality (Fig. 4 *C* and *D*). Resultantly, the cell failed to move inside the "blue square" (Fig. 4*B* and Movie S3). In addition to abrogating front–rear coordination, nimodipine also dramatically decreased migration velocity (control: 15.2 μm/h; +nimodipine: 3.4 μm/h). Interestingly,

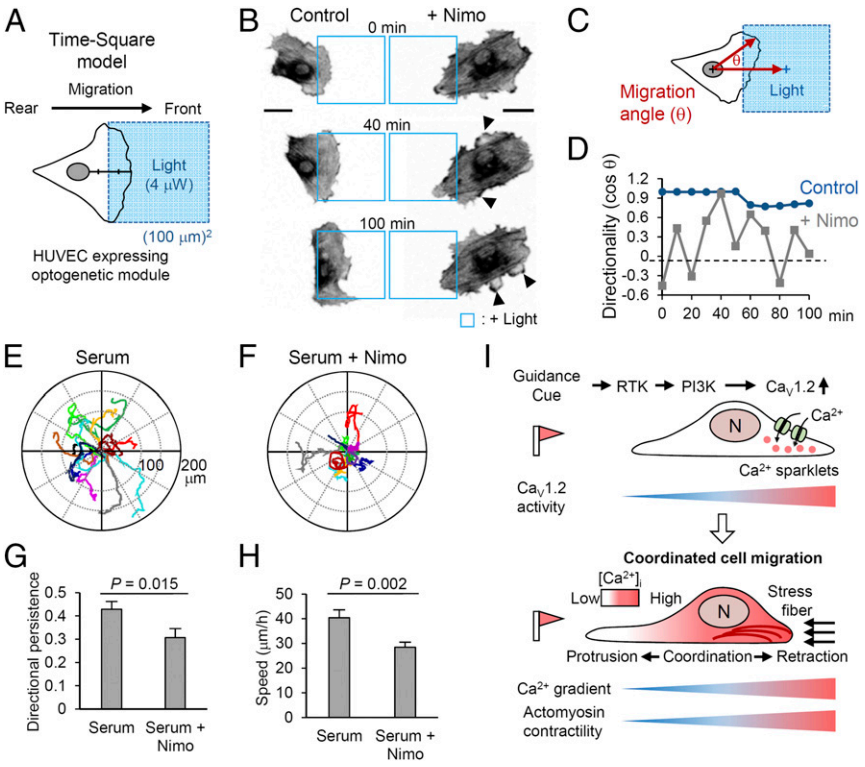

Fig. 4. Effects of the front-to-rear Ca^{2+} gradient on motile pattern. (*A*) Basic scheme of the time-square model. A square-shaped blue light (blue box) illuminates an area in the anterior half (midpoint between front edge and border of nucleus) of HUVECs expressing an optogenetic module. See *SI Materials and Methods*. (*B*) Lifeact images (inverted contrast) of directionally migrating HUVECs under optoFGFR1 guidance (time-square model), with and without nimodipine treatment. Blue squares represent the illuminated region; arrowheads indicate lateral lamellipodia. (*C*) Schematic illustration of the method for determining migration angle (θ), where θ is the angle between the migrating direction and the central axis of the illuminated region. (*D*) Time course of the directionality (cos θ) of an optoFGFR1-expressing HUVEC (blue) and the cell treated with nimodipine (gray). (*E* and *F*) Migrating paths of HUVECs (10 h) in serum-supplemented media with and without nimodipine treatment. (*G* and *H*) Directional persistence (displacement/total path) and speed of migrating HUVECs. $n = 50$ (serum) and $n = 40$ (serum + Nimo). Data are represented as mean ± SEM, two-tailed *t* test. (*I*) Proposed model of front–rear coordination in directed cell migration. Polarized $Ca_V1.2$ activity establishes a Ca^{2+} gradient that maintains cell polarity by inducing actomyosin contractility in the rear part of the migrating cell. (Scale bars: 20 μm.)

these effects of nimodipine were markedly rescued by coexpression of an MLC-phosphomimetic mutant (MRLC2-DD), which enhances MLCK downstream activity (Fig. S7 *A* and *B*). Thus, this exquisitely designed optogenetic model clearly revealed that the Ca^{2+} gradient acts as a crucial mediator of sustained directionality as well as migration efficiency through modulation of actomyosin contractility.

We showed that active retraction of the rear part in response to localized illumination only occurs in cells expressing optoFGFR1, but the retraction was less active in those expressing PA-Rac1 (Fig. 1 *B–D*). This, taken together with the observed rescue of nimodipine-impaired directional migration, suggests that coexpression of MRLC2-DD could alter the motile pattern of PA-Rac1–expressing cells to yield rear contractility similar to that of optoFGFR1-expressing cells. In the time-square model, cells coexpressing PA-Rac1 and MRLC2-DD showed an elongated morphology and efficiently moved into the illuminated region with active rear contraction, whereas cells expressing PA-Rac1 only showed delayed migration with a dragging rear part (Fig. S7*C*). Notably, the retractile force produced by MRLC2-DD propelled forward movement of the nucleus (nucleokinesis), reflecting efficient bodily movement of the cell. We also found that the nucleus-to-trailing edge (N–T) distance was remarkably shortened (−37.29 μm/h) in MRLC2-DD coexpressing cells, providing further support for rear retraction (Fig. S7*D*). Coexpression of MRLC2-DD also significantly increased migration velocity (13.0 μm/h) compared with cells expressing PA-Rac1 only (4.7 μm/h) (Fig. S7*E*). These results highlight the importance of the traction force driven by actomyosin crosslinking of the rear part in front–rear coordination during directional cell migration. Finally, we tracked the autonomous movement (chemokinesis) of HUVECs under serum-supplemented conditions, and evaluated their patterns upon nimodipine treatment. Interestingly, whereas normal cells moved along a linear path, Ca_V channel-blocked cells showed a winding migration pattern, indicating frequent changes of direction (Fig. 4 *E* and *F* and Movie S4). This different migration mode is clearly evidenced by a significant decrease in directional persistence (displacement/total path, serum: 0.43; serum + nimodipine: 0.31) and speed (serum: 40.4 μm/h; serum + nimodipine: 28.4 μm/h) in nimodipine-treated cells (Fig. 4 *G* and *H*).

Collectively, the results of diverse migration studies clearly show that an asymmetric Ca^{2+} distribution coordinates directional cell movement by maintaining actomyosin contractility in the rear part, which is crucial for stabilizing the directional persistence of migrating cells (Fig. 4*I*).

Discussion

Our study introduces the spatial roles of Ca^{2+} sparklets derived from $Ca_V1.2$ channels in coordinating endothelial cell migration. Various excitable cells heterogeneously express L-type Ca_V channels, and the biological functions of these channels, such as neuronal transmission and muscle contraction, have been extensively studied. However, the function and regulatory mechanism of L-type Ca_V channels in nonexcitable cells has rarely been studied, especially in mesenchymal cell migration. L-type Ca_V channels are up-/down-regulated via multiple signaling mediators induced by extracellular stimuli (32). In particular, studies of RTK-mediated Ca_V channel regulation have reported conflicting results—tyrosine kinase-dependent increase or decrease in L-type Ca_V channel currents—depending on biological contexts (33, 34). In the current study, we observed that the PLCγ–PKC cascade and lipid modulation by PI3K, two representative downstream pathways of RTK, act as dominant inhibitory and triggering signals for Ca^{2+} sparklets, respectively. Intriguingly, these RTK downstream pathways elicit site-specific effects through signal coupling (possibly including cross-talk) in leading or trailing parts of a single cell, yielding a rear-concentrated pattern of Ca^{2+} sparklets (Fig. S3*K*). However, dissecting the complete mechanism will require further investigation of additional signaling components involved in patterning front-rear Ca^{2+} signals in migrating cells.

We also demonstrated that the localized Ca^{2+} sparklets from L-type Ca_V channel are crucial mediators in the establishment of front-to-rear increasing Ca^{2+} gradients. During directional migration, an increasing front-to-rear pattern of intracellular Ca^{2+}

level has been commonly observed in diverse cell types, but the mechanism by which the Ca^{2+} gradient is generated is largely unknown. Evidence to date has shown that local Ca^{2+} transients in many types of migrating cells, including stretched keratocytes (5) and fibroblasts (4) as well as collectively migrating HUVECs (28, 35), are actually located in the front region of the cell, creating challenges for defining front-to-rear Ca^{2+} gradients. In this study, we directly visualized Ca^{2+} sparklets, which were mainly located in the rear part of the cells, by applying an optical guidance model and showed that blocking L-type Ca_V channels rapidly abolished the Ca^{2+} gradient and reduced the directional persistency of the cells. These findings provide clear evidence for the generating mechanism of front–rear Ca^{2+} gradients, suggesting a novel role of Ca_V channels in the directional migration of nonexcitable cells.

In this work, we have also sought to provide representative guidelines for using optogenetic toolkit in biological studies, especially in directed cell migration. Previously used methods for recapitulating directional migration require complex machinery or are not easily reversible or repeatable. The optogenetic approach provides an elegant experimental strategy that is suitable for implementation on a conventional microscope setup providing subsecond and submicrometer precision. Moreover, optogenetic tools are uniquely capable of modulating specific signaling nodes in a specified region and at specific time points, offering an unparalleled method for assessing cellular responses between activated and unactivated regions of a single cell (10, 36). In our studies, we perturbed individual signaling nodes comprising the RTK signaling cascade using optoFGFR1 or PA-Rac1 and assessed cellular movement. This comparative approach proved decisive in revealing that the efficiency of front–rear coordination depends on a different hierarchy of signaling: optoFGFR1 produces more robust rear contraction compared with the PA-Rac1 (Fig. 1 *B–D*). In addition, directly activating the PI3K cascade using light-inducible PI3K enabled us to elucidate a core signaling requirement for the induction of Ca^{2+} sparklets (Fig. S3 *B* and *C*). The direct access to individual signaling nodes provided by optogenetic tools is a powerful asset in dissecting the mechanisms underlying biological events in which multiple signaling pathways are orchestrated. Collectively, these superior properties—excellent spatiotemporal resolution and direct signal accessibility—clearly justify the use of an optogenetic toolkit in the diverse biological fields.

Our study results, taken together, establish a clear pathway that links local Ca^{2+} signals and front–rear coordination during directed cell migration.

Materials and Methods

HUVECs (Gibco) were transfected using the Neon Transfection System (Invitrogen). Transfected cells were plated on plastic-bottom 96-well plates (Ibidi) coated with collagen solution (Advanced Biomatrix). Live-cell imaging was conducted using a Nikon A1R confocal microscope. Optogenetic modules were stimulated by photoactivation using a 488-nm laser emitted through a Galvano scanner (Nikon). Detailed experimental procedures are provided in *SI Materials and Methods*.

ACKNOWLEDGMENTS. We thank Y. J. Jo (KAIST) for brilliant video processing algorithms. This work was supported by the Institute for Basic Science (IBS-R001-G1) and KAIST Institute for the BioCentury, Republic of Korea.

1. Ridley AJ, et al. (2003) Cell migration: Integrating signals from front to back. *Science* 302(5651):1704–1709.
2. Petrie RJ, Doyle AD, Yamada KM (2009) Random versus directionally persistent cell migration. *Nat Rev Mol Cell Biol* 10(8):538–549.
3. Tadross MR, Dick IE, Yue DT (2008) Mechanism of local and global Ca2+ sensing by calmodulin in complex with a Ca2+ channel. *Cell* 133(7):1228–1240.
4. Wei C, et al. (2009) Calcium flickers steer cell migration. *Nature* 457(7231):901–905.
5. Lee J, Ishihara A, Oxford G, Johnson B, Jacobson K (1999) Regulation of cell movement is mediated by stretch-activated calcium channels. *Nature* 400(6742):382–386.
6. Yang S, Huang XY (2005) Ca2+ influx through L-type Ca2+ channels controls the trailing tail contraction in growth factor-induced fibroblast cell migration. *J Biol Chem* 280(29):27130–27137.
7. Wu YI, et al. (2009) A genetically encoded photoactivatable Rac controls the motility of living cells. *Nature* 461(7260):104–108.
8. Levskaya A, Weiner OD, Lim WA, Voigt CA (2009) Spatiotemporal control of cell signalling using a light-switchable protein interaction. *Nature* 461(7266):997–1001.
9. Kennedy MJ, et al. (2010) Rapid blue-light-mediated induction of protein interactions in living cells. *Nat Methods* 7(12):973–975.
10. Tischer D, Weiner OD (2014) Illuminating cell signalling with optogenetic tools. *Nat Rev Mol Cell Biol* 15(8):551–558.
11. Idevall-Hagren O, Dickson EJ, Hille B, Toomre DK, De Camilli P (2012) Optogenetic control of phosphoinositide metabolism. *Proc Natl Acad Sci USA* 109(35):E2316–E2323.
12. Kim N, et al. (2014) Spatiotemporal control of fibroblast growth factor receptor signals by blue light. *Chem Biol* 21(7):903–912.
13. Riedl J, et al. (2008) Lifeact: A versatile marker to visualize F-actin. *Nat Methods* 5(7): 605–607.
14. Wilson CA, et al. (2010) Myosin II contributes to cell-scale actin network treadmilling through network disassembly. *Nature* 465(7296):373–377.
15. Berridge MJ, Bootman MD, Roderick HL (2003) Calcium signalling: Dynamics, homeostasis and remodelling. *Nat Rev Mol Cell Biol* 4(7):517–529.
16. Zhao Y, et al. (2011) An expanded palette of genetically encoded Ca(2)(+) indicators. *Science* 333(6051):1888–1891.
17. Shigetomi E, Kracun S, Sofroniew MV, Khakh BS (2010) A genetically targeted optical sensor to monitor calcium signals in astrocyte processes. *Nat Neurosci* 13(6):759–766.
18. Cheng H, Lederer WJ (2008) Calcium sparks. *Physiol Rev* 88(4):1491–1545.
19. Ertel EA, et al. (2000) Nomenclature of voltage-gated calcium channels. *Neuron* 25(3): 533–535.
20. Le Blanc C, et al. (2004) Regulation of vascular L-type Ca2+ channels by phosphatidylinositol 3,4,5-trisphosphate. *Circ Res* 95(3):300–307.
21. Viard P, et al. (2004) PI3K promotes voltage-dependent calcium channel trafficking to the plasma membrane. *Nat Neurosci* 7(9):939–946.
22. Haugh JM, Codazzi F, Teruel M, Meyer T (2000) Spatial sensing in fibroblasts mediated by 3′ phosphoinositides. *J Cell Biol* 151(6):1269–1280.
23. van Rheenen J, Jalink K (2002) Agonist-induced PIP(2) hydrolysis inhibits cortical actin dynamics: Regulation at a global but not at a micrometer scale. *Mol Biol Cell* 13(9): 3257–3267.
24. Woo SH, Lee CO (1999) Role of PKC in the effects of alpha1-adrenergic stimulation on Ca2+ transients, contraction and Ca2+ current in guinea-pig ventricular myocytes. *Pflugers Arch* 437(3):335–344.
25. Zhang S, Hirano Y, Hiraoka M (1995) Arginine vasopressin-induced potentiation of unitary L-type Ca2+ channel current in guinea pig ventricular myocytes. *Circ Res* 76(4): 592–599.
26. Shen Q, Rigor RR, Pivetti CD, Wu MH, Yuan SY (2010) Myosin light chain kinase in microvascular endothelial barrier function. *Cardiovasc Res* 87(2):272–280.
27. Brundage RA, Fogarty KE, Tuft RA, Fay FS (1991) Calcium gradients underlying polarization and chemotaxis of eosinophils. *Science* 254(5032):703–706.
28. Tsai FC, et al. (2014) A polarized Ca2+, diacylglycerol and STIM1 signalling system regulates directed cell migration. *Nat Cell Biol* 16(2):133–144.
29. Lipp P, Niggli E (1993) Ratiometric confocal Ca(2+)-measurements with visible wavelength indicators in isolated cardiac myocytes. *Cell Calcium* 14(5):359–372.
30. Inoue T, Heo WD, Grimley JS, Wandless TJ, Meyer T (2005) An inducible translocation strategy to rapidly activate and inhibit small GTPase signaling pathways. *Nat Methods* 2(6):415–418.
31. Suh BC, Inoue T, Meyer T, Hille B (2006) Rapid chemically induced changes of PtdIns (4,5)P2 gate KCNQ ion channels. *Science* 314(5804):1454–1457.
32. Kamp TJ, Hell JW (2000) Regulation of cardiac L-type calcium channels by protein kinase A and protein kinase C. *Circ Res* 87(12):1095–1102.
33. Blair LA, Marshall J (1997) IGF-1 modulates N and L calcium channels in a PI 3-kinase-dependent manner. *Neuron* 19(2):421–429.
34. Hinkle PM, Nelson EJ, Haymes AA (1993) Regulation of L-type voltage-gated calcium channels by epidermal growth factor. *Endocrinology* 133(1):271–276.
35. Tsai FC, Meyer T (2012) Ca2+ pulses control local cycles of lamellipodia retraction and adhesion along the front of migrating cells. *Curr Biol* 22(9):837–842.
36. Toettcher JE, Weiner OD, Lim WA (2013) Using optogenetics to interrogate the dynamic control of signal transmission by the Ras/Erk module. *Cell* 155(6):1422–1434.
37. Shcherbakova DM, Verkhusha VV (2013) Near-infrared fluorescent proteins for multicolor in vivo imaging. *Nat Methods* 10(8):751–754.
38. Dulyaninova NG, Patskovsky YV, Bresnick AR (2004) The N-terminus of the long MLCK induces a disruption in normal spindle morphology and metaphase arrest. *J Cell Sci* 117(Pt 8):1481–1493.
39. Moffat J, et al. (2006) A lentiviral RNAi library for human and mouse genes applied to an arrayed viral high-content screen. *Cell* 124(6):1283–1298.
40. Lee S, et al. (2014) Reversible protein inactivation by optogenetic trapping in cells. *Nat Methods* 11(6):633–636.
41. Vicente-Manzanares M, Koach MA, Whitmore L, Lamers ML, Horwitz AF (2008) Segregation and activation of myosin IIB creates a rear in migrating cells. *J Cell Biol* 183(3):543–554.
42. Dudley RA, et al. (1985) Guidelines for immunoassay data processing. *Clin Chem* 31(8): 1264–1271.
43. Pearman CM (2014) An Excel-based implementation of the spectral method of action potential alternans analysis. *Physiol Rep* 2(12) pii: e12194.